VIRUS EVOLUTION

Virus Evolution, 2022, **8(2)**, 1–12
DOI: https://doi.org/10.1093/ve/veac091
Advance access publication date: 28 September 2022
Research Article

Accumulation of copy-back viral genomes during respiratory syncytial virus infection is preceded by diversification of the copy-back viral genome population followed by selection

Sébastien A. Felt,[†] Emna Achouri, Sydney R. Faber, and Carolina B. López[*,‡]

Department of Molecular Microbiology and Center for Women Infectious Disease Research, Washington University School of Medicine, St Louis, MO 63108, USA
[†]https://orcid.org/0000-0003-2942-7203
[‡]https://orcid.org/0000-0002-7669-6572
*Corresponding author: E-mail: clopezzalaquett@wustl.edu

Abstract

RNA viruses generate nonstandard viral genomes during their replication, including viral genomes of the copy-back (cbVGs) type that cannot replicate in the absence of a standard virus. cbVGs play a crucial role in shaping virus infection outcomes due to their ability to interfere with virus replication and induce strong immune responses. However, despite their critical role during infection, the principles that drive the selection and evolution of cbVGs within a virus population are poorly understood. As cbVGs are dependent on the virus replication machinery to be generated and replicated, we hypothesized that host factors that affect virus replication exert selective pressure on cbVGs and drive their evolution within a virus population. To test this hypothesis, we used respiratory syncytial virus (RSV) as a model and took an experimental evolution approach by serially passaging RSV in immune-competent human lung adenocarcinoma A549 control and immune-deficient A549 Signal transducer and activator of transcription 1 (STAT1) KO cells, which allow higher levels of virus replication. As predicted, we observed that virus populations accumulated higher amounts of cbVGs in the more permissive A549 STAT1 KO cells over time; however, unexpectedly, the predominant cbVG species after passages in the two conditions were different. While A549 STAT1 KO cells accumulated relatively short cbVGs, A549 control cells mainly contained cbVGs of much longer predicted size, which have not been described previously. These long cbVGs were predominant at first in both cell lines *in vitro* and the predominant ones observed in samples from RSV-infected patients. Although sustained high replication levels are associated with cbVG generation and accumulation, our data show that sustained high levels of virus replication are critical for cbVG population diversification, a process that precedes the generation of shorter cbVGs that selectively accumulate over time. Taken together, we show that selection and evolution of cbVGs within a virus population are shaped by how resistant or permissive a host is to RSV.

Key words: respiratory syncytial virus; copy-back viral genomes; experimental evolution.

1. Introduction

The ability of RNA viruses to rapidly evolve is a major concern for public health due to the potential emergence of virus variants with enhanced pathogenicity (Carrasco-Hernandez et al. 2017). It is, therefore, of critical importance to understand the principles that drive virus evolution. An RNA virus consists of communities of standard viral genomes and nonstandard viral genomes, such as copy-back viral genomes (cbVGs), which are generated during virus replication (Vignuzzi and Lopez 2019). Of note, cbVGs are also known as 'defective viral genomes' or DVGs. Since the word 'defective' may give the wrong impression that cbVGs have no function during a viral infection, we herein call them cbVGs, as these kinds of genomes do play important roles during infection (Vignuzzi and Lopez 2019; González-Aparicio, López, and Felt 2022).

cbVGs are generated when the polymerase detaches from the template strand at a break point and resumes elongation at a downstream rejoin point creating a complementary end to the 5′ end of the nascent genome (Kolakofsky 1976; Lazzarini, Keene, and Schubert 1981; Vignuzzi and Lopez 2019). cbVGs are usually shorter than standard viral genomes, and their flanking trailer promoters have a higher affinity for the viral polymerase than the leader promoter present at the 3′ end of the standard viral genome, thereby providing a replication advantage to cbVGs (Rao and Huang 1982; Li and Pattnaik 1997). This advantage in replication can lead to the accumulation (significant increase) of shorter cbVGs within virus populations. cbVGs depend on standard viral genomes to be generated and replicated. Many cbVGs are packaged and released from the infected cell and can infect new host cells affecting the interaction of the virus with the host

(Lazzarini, Keene, and Schubert 1981; Vignuzzi and Lopez 2019). cbVGs can inhibit standard viral genome replication by competing for the virus replication machinery or by inducing innate immune signaling pathways (Henle and Henle 1943; Strahle, Garcin, and Kolakofsky 2006; Tapia et al. 2013; Sun et al. 2015). Despite the critical role of cbVGs in shaping the infection outcome, most RNA virus evolution studies only consider standard viral genomes. As a result of this, the principles that drive the selection and evolution of cbVGs within a virus population are poorly understood.

As cbVGs depend on the virus replication machinery to be generated and amplified, we hypothesized that host factors that affect virus replication exert selective pressure on cbVGs and drive their evolution within a virus population. To test this hypothesis, we used the non-segmented negative-sense RNA virus respiratory syncytial virus (RSV) as a model because RSV generates many cbVGs during infection *in vitro* and *in vivo* (Treuhaft and Beem 1982; Sun et al. 2015; Felt et al. 2021). RSV cbVGs stimulate Mitochondrial antiviral-signaling (MAVS) signaling during infection, which leads to the production of antiviral type I and III interferons (IFNs) (Sun et al. 2015). This antiviral response is dependent on cbVGs triggering the intracellular viral sensors retinoic acid-inducible gene I (RIG-I)-like receptors, as has been shown for many non-segmented negative-sense RNA viruses (Strahle et al. 2007; Yount et al. 2008; Baum et al. 2010; Runge et al. 2014; Xu et al. 2015; Ho et al. 2016; Mura et al. 2017; Linder et al. 2021). The expression of type I and III IFNs leads to the activation of STAT1, which is followed by the production of hundreds of proteins that interfere with virus replication (Mesev, LeDesma, and Ploss 2019). Interestingly, recently, it has been shown that viruses can activate STAT1 even earlier independent of IFNs through a RIG-I/MAVS/Spleen tyrosine kinase (Syk) pathway further establishing STAT1 as an important antiviral protein (Liu et al. 2021). *In vivo*, RSV can replicate to higher levels in STAT1-knockout mice compared to wild-type mice (Durbin et al. 2002; Hashimoto et al. 2005; Stier et al. 2017). Based on these studies, we decided to test if STAT1 exerts selective pressure on RSV cbVGs and drive their evolution. Specifically, we took an experimental evolution approach and serially passaged RSV using a fixed-volume or a fixed multiplicity of infection (MOI) in immune-competent A549 control cells or in immune-deficient A549 STAT1 KO cells. As RSV also generates cbVGs in infected patients (Felt et al. 2021; Sun et al. 2015), we also analyzed cbVGs in nasal washes from RSV-infected pediatric patients to assess what cbVGs are selected for during natural infections.

To detect cbVGs in RNAseq data, we used an updated version of our previously published Viral Opensource DVG Key Algorithm (VODKA) (Sun et al. 2019), called VODKA2, which identifies cbVG reads based on their alignment to unique junction sequences that contain a break and rejoin point. Predicted cbVG species sizes can then be calculated based on the break and rejoin points. Our study revealed that the diversity of cbVGs generated is much larger than previously thought. We found that cbVGs of longer predicted sizes that have not been described previously are predominant at first *in vitro* and the major cbVGs present in samples from RSV-infected patients. Furthermore, sustained high virus replication levels led to cbVG population diversification that preceded the generation and selective accumulation of shorter cbVGs.

2. Methodology

2.1 Cells and viruses

A549 control cells, A549 STAT1 KO cells, and HEp2 cells (HeLa-derived human epithelial cells, ATCC CCL23) were cultured at 5 per cent CO_2 and 37°C in Dulbecco's modified Eagle's medium supplemented with 10 per cent fetal bovine serum, 1 mM sodium pyruvate, 2 mM L-glutamine, and 50 mg/ml gentamicin. The A549 Clustered Regularly Interspaced Short Palindromic Repeats cell lines were kindly provided by Dr. Susan Weiss (University of Pennsylvania) and have been previously characterized (Xu et al. 2017; Whelan et al. 2019). All cell lines were treated with *Mycoplasma* removal agent (MP Biomedicals) and routinely tested for *Mycoplasma* before use. RSV A2 was obtained from ATCC (#VR-1540) and amplified in Hep2 cells at a low MOI of 0.01 to generate RSV stocks with low cbVG contents (Sun and Lopez 2016). We used these stocks as parental (P0) virus stocks for our experiments.

2.2 Passaging experiments

In fixed-volume passaging experiments, for the first passage, A549 control and STAT1 KO cells were infected at an MOI of ten with an RSV stock with a low cbVG content (P0) to focus mainly on *de novo* generation of cbVGs. We chose this MOI as higher MOIs favor the accumulation of nonstandard viral genomes, including cbVGs, in virus populations (Von Magnus 1951; 1954; Kingsbury, Portner, and Darlington 1970; Stampfer, Baltimore, and Huang 1971; Huang 1973; Thompson and Yin 2010; Sun and Lopez 2016; Welch et al. 2020). Two days postinfection (before too many cells start dying (Collins, Fearns, and Graham 2013)), cells were collected and centrifuged for five minutes at 280 × *g* to separate supernatant from cells. Most of the supernatant was transferred to a new tube and kept on ice to preserve viral particles. The remaining supernatant was left to cover the cell pellet to make sure that the cells did not dry. As most RSV particles remain attached to cells (Collins, Fearns, and Graham 2013), three freeze/thaw (dry ice/ethanol + 37°C water bath) cycles were performed on the cell pellet to release virus particles. Pellets were vortexed after each freeze/thaw cycle to further increase virus particle release. Pellets were then centrifuged for five minutes at 280 × *g* to separate cell debris from supernatant with released viral particles. Supernatant from freeze/thaw cycles was then mixed with supernatant that was kept on ice and 36 ul, which represents ∼1/25th of the total mixed supernatant, was then used to infect the next round of fresh cells (Passage 2). These procedures and volume were kept consistent throughout the remaining passages. We chose a ratio of ∼1/25 as in a previous study, it was shown to lead to accumulation of non-standard viral genomes (Williams et al. 2016). At each passage, the remaining supernatant was snap frozen in dry ice/ethanol to preserve viral particles for downstream analysis (titration and RNAseq/VODKA2 analysis). It is important to note that, in addition to viral particles, the samples also contain unpackaged viral RNAs.

For the fixed-MOI passaging experiment, A549 control and STAT1 KO cells were initially infected at an MOI of 0.1 or 10 with an RSV stock with a low cbVG content (P0). The steps between each passage and preservation of samples were performed such as for the fixed-volume experiment. However, supernatants were tittered in between each passage to maintain the same MOI throughout the ten passages. For the fixed MOI of ten experiments, an MOI of ten was maintained if titer and volumes allowed it. For the first six passages, it was possible to use an MOI of ten; however, for Passages 7, 8, 9, and 10, the MOIs were reduced to 5, 8, 5, and 5, respectively.

2.3 Titration

Supernatants were tittered by Median Tissue Culture Infectious Dose ($TCID_{50}$) on Hep2 cells to assess the amount of infectious

viral particles as previously published (Sun and Lopez 2016). Briefly, supernatants were serially diluted, added on Hep2 cells, and incubated for 4–5 days, and after addition of crystal violet, the last dilution with cytopathic effect was determined to calculate the $TCID_{50}$.

2.4 Nasopharyngeal aspirates

Nasopharyngeal aspirates from pediatric patients were obtained from the Children's Hospital of Philadelphia (CHOP). The CHOP cohort was previously described in detail (Felt et al. 2021). All samples used were banked samples obtained as part of standard testing of patients. Samples were deidentified and sent to our laboratory for RNA extraction and cbVG detection.

2.5 RNAseq

Total RNA was extracted using TRIzol LS (Invitrogen). RNA quality was assessed using an Agilent TapeStation or Bioanalyzer (Agilent Technologies) before complementary deoxyribonucleic acid (cDNA) library preparation. All samples were prepared using the Illumina Non-Stranded Total RNA Library Prep Kit with Ribo-Zero Gold. The only exceptions were the clinical samples, which were prepared using the Sigma SeqPlex RNA Amplification Kit, and the samples shown in Fig. S3, which were prepared using the Illumina TruSeq Stranded Total RNA Library Prep Kit with Ribo-Zero Gold. All samples were run on a NovaSeq 6000 to generate 150-bp, paired-end reads, resulting in ∼33–62 million reads per sample. The only exceptions were samples shown in Fig. S3, which were run on an Illumina NextSeq 500 to generate 75-bp, single-end reads, resulting in ∼45–72 million reads per sample. Only R1 reads were used for analysis as many reads in R2 were duplicates. The average Phred quality score of samples ranged between 34.7 and 36.1. Raw RNAseq data from Figs S3 and S5A were used in previous studies (Xu et al. 2017; Sun et al. 2019).

2.6 VODKA2

After trimming sequencing adapters (Illumina Universal Adapter—AGATCGGAAGAG, https://support.illumina.com/) from the 3′ end of the reads using Cutadapt (DOI: 10.14806/ej.17.1.200) and removing all reads aligned to the human genome (GRCh38, GRC website) with Bowtie2 (https://doi.org/10.1038/nmeth.1923), an updated version of VODKA (VODKA2.0 beta, https://github.com/eachouri/VODKA2/tree/main/VODKA2-v2.0b-master) was used to detect cbVG junction reads derived from the entire viral genome (*in vitro* reference genome KT992094.1 and clinical samples reference genome KC731482.1). We only focused on cbVGs generated from the 5′ end of the viral genome, which are the best described in the literature (Vignuzzi and Lopez 2019). Briefly, VODKA2.0 beta first runs a Bowtie2 alignment of the reads against a database representing all theoretical cbVGs potentially present in the data set (KT992094.1: 231,298,470 possibilities and KC731482.1: 231,541,872 possibilities). Reads are removed unless they map across break and rejoin junction sequences with at least 15 bp of mapped segment on each side. This is followed by an extra filtering step based on the Basic Local Alignment Search Tool (Blastn v.2.11.0, https://doi.org/10.1016/S0022-2836(05)80360-2) alignment of the predicted break and rejoin junction sequences against the virus reference genome (BLAST options: '-word_size 11 -gapopen 5 -gapextend 2 -penalty –3 -reward 2 -evalue 0.001 -perc_identity 0.1'). Only sequences with two alignment ranges reported on opposite strands of the reference genome are considered cbVG reads. Sequences with BLAST alignment positions that are not consistent with the initial Bowtie2 alignment are discarded. An extended report is then generated, including in particular the aggregation of cbVG junction reads into 'species', i.e., junction reads leading to cbVGs of the exactly same theoretical size but with break and rejoin occurring within a range of ±5 nucleotides. 'Species' with only one read were removed from analysis. Break and rejoin positions from VODKA2.0 beta were used to calculate the predicted size of cbVGs [(break position – genome size) + (rejoin position – genome size) + 2].

2.7 Statistical analysis

Statistical analyses were performed as indicated in each figure legend using GraphPad Prism v.9.

3. Results

3.1 cbVGs accumulate to higher levels after twenty passages in A549 STAT1 KO cells than in A549 control cells

To examine the evolution of cbVG populations and selection of cbVG species, we passaged a fixed volume of supernatant from RSV-infected cells twenty times in A549 control cells or A549 STAT1 KO cells (Fig. 1A). To assess *de novo* generation of cbVGs, we started with a parental virus stock (Passage 0, P0) that contained low levels of cbVGs. We confirmed the low cbVG content by our previously established reverse transcription polymerase chain reaction (RT-PCR) method and RNAseq/VODKA2 pipeline (Table 1) (Sun et al. 2015; 2019). We carried out three experimental evolution replicates (three lineages) for each cell line and repeated this experiment independently three times. For simplicity in visual representation, one representative repeat is shown throughout. As expected, RSV replication, as measured by titer, was overall higher in A549 STAT1 KO cells than in A549 control cells, at least for the first fourteen passages, for all three lineages (Fig. 1B). RSV replication dropped to very low levels for several passages in A549 control cells, whereas RSV replication was maintained to high levels throughout the experiment in A549 STAT1 KO cells (Fig. 1B). To assess how cbVGs evolved in these two cell lines, we performed RNAseq followed by analysis using VODKA2 for the detection of cbVGs in P0 and in Passage 20. cbVG junction reads were detected in all samples, and cbVG content increased significantly more in virus populations passaged in A549 STAT1 KO cells (S1–S3) than in A549 control cells (C1–C3) (Table 1 and Fig. 1C). These data demonstrate that an environment that does not allow RSV to maintain high replication levels, such as A549 control cells, impedes cbVG accumulation. However, an environment that allows RSV to maintain high replication levels, such as A549 STAT1 KO cells, promotes cbVG accumulation. This is consistent with the literature as most studies use permissive cells or cells with innate immune defects to generate viral stocks with a high cbVG content (Santak et al. 2015; Sun and Lopez 2016; Welch et al. 2020; Tilston-Lunel et al. 2021).

3.2 Short cbVGs accumulate after twenty passages in A549 STAT1 KO cells but not in A549 control cells

We next determined the break (where the polymerase fell off) and rejoin (where the polymerase reattached) genome position of the cbVGs present in each sample (Fig. S1A). As cbVGs unique sequence and size can be predicted by its break/rejoin positions, we used these data to determine if different cbVG species were present in our samples. In previous studies, we set up VODKA to detect cbVGs generated only on the last 3000 bp of the RSV genome as we were only interested in the cbVG species with the most reads (Sun et al. 2019). However, in this study, we assessed the entire

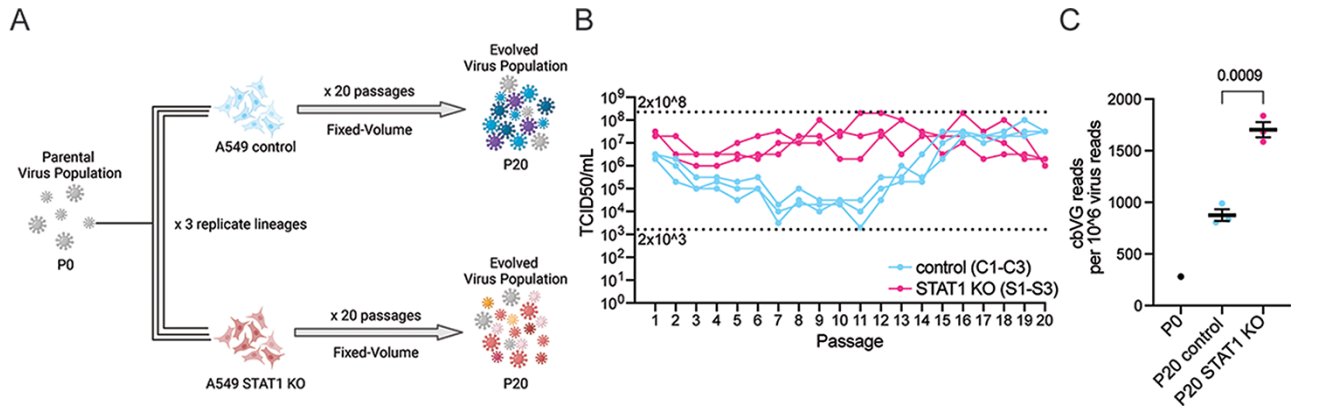

Figure 1. Experimental evolution design and detection of infectious viral particles and cbVGs. (A) Schematic of experimental evolution experiment. (B) $TCID_{50}$ assay was performed on Hep2 cells for all samples. Dashed lines indicate the minimum and maximum $TCID_{50}$/ml values reached in the experiment. (C) cbVG reads detected by VODKA2 were normalized per 10^6 virus reads. Data are shown as mean ± SEM. Significant *P* value for the two-tailed unpaired *t* test between A549 control and A549 STAT1 KO ($n = 3$ lineages) is indicated.

Table 1. RNAseq/VODKA2 data of parental virus population and Passage 20 virus populations.

Sample	Non-junction reads (=virus reads)	Junction reads (=cbVG reads)	Normalized cbVG reads per 10^6 virus reads	Median break position (IQR)	Median rejoin position (IQR)	Median predicted cbVG size in bp (IQR)
P0	1,823,842	513	281	3,480 (1927–7289)	3,658 (1967–7636)	2,3345 (15489–26534)
C1	3,967,544	3,923	989	2,779 (1577–4412)	2,929 (1625–4506)	24,701 (21575–27258)
C2	2,600,483	2,167	833	2,828 (1581–4417)	2,929 (1695–4738)	24,680 (21050–27155)
C3	3,407,084	2,743	805	2,828 (1581–4417)	2,945 (1698–4740)	24,640 (21468–27155)
S1	358,301	603	1,683	1,4596 (2786–15036)	15,058 (2905–15175)	794 (236–24757)
S1	247,193	393	1,590	11,751 (1831–14724)	11,769 (1926–15048)	6,931 (675–26693)
S1	339,583	624	1,838	11,341 (2353–14895)	11,415 (2379–15182)	7,693 (370–25721)

IQR = interquartile range

cbVG population, and thus, we set up VODKA2 to identify cbVG junction reads generated through the entire RSV genome.

We observed that more cbVGs in virus populations from A549 STAT1 KO cells had break and rejoin positions in the last 3000 bp of the RSV genome (dashed box) corresponding to cbVG species of predicted shorter size as compared to virus populations from A549 control cells (Fig. 2A). This is consistent with our previous study where we showed that RSV populations with high cbVG content had break and rejoin hotspots toward the trailer end of the RSV genome (Sun et al. 2019). However, by running VODKA2 on the entire genome, we discovered novel cbVG species with break and rejoin positions outside the 3000 bp range and many with predicted sizes longer than the genome (Figs 2A and S1B). It is also important to note that most cbVG species detected in P20 were not present in P0. We found that between 90.5 per cent and 95.9 per cent of cbVG species in the six P20 cbVG populations were *de novo* generated rather than being carried over from P0.

To consider variability and stochasticity in cbVG species generation and accumulation, we also plotted the median break (Fig. 2B), rejoin (Fig. 2C), and predicted size (Fig. 2D) for each lineage (Table 1). The median values of the three lineages in each condition were similar, and the differences observed in break, rejoin, and predicted size in different conditions were statistically different (Fig. 2B–D). Finally, we observed that in each A549 STAT1 KO cells, lineage (S1–S3) cbVG species of short sizes started to dominate the cbVG population after twenty passages (Fig. 2A and E). Taken together, our data show that cbVG populations are diverse, that cbVGs are generated across the entire genome, and that short cbVG species are selected for in permissive A549 STAT1 KO cells. This selection was not observed in virus populations passaged in more resistant A549 control cells. Instead, long cbVGs remained predominant, and no individual longer cbVG species outcompeted the others.

3.3 Longer predicted cbVGs are predominant in nasal washes of hospitalized RSV-infected pediatric patients

We detected predominantly cbVG species of longer predicted sizes in virus populations from A549 control cells (Fig. 2A). Longer predicted cbVG species were also present in virus populations from A549 STAT1 KO cells; however, they were outcompeted by shorter cbVG species (Fig. 2A and E). In both cell lines, longer predicted cbVGs species had fewer reads, which indicates that they do not accumulate as much as the shorter cbVG species (Fig. 2A). To determine whether long cbVGs are of biological significance, we sought to assess if longer predicted cbVGs could be detected during natural infections. We have previously shown that detection of RSV cbVGs in nasal secretions of infected patients is associated with distinct clinical outcomes. To determine what cbVG species are generated in natural RSV infections, we chose six representative samples from RSV-infected pediatric patients, which were previously confirmed to contain cbVGs by our pan-cbVG

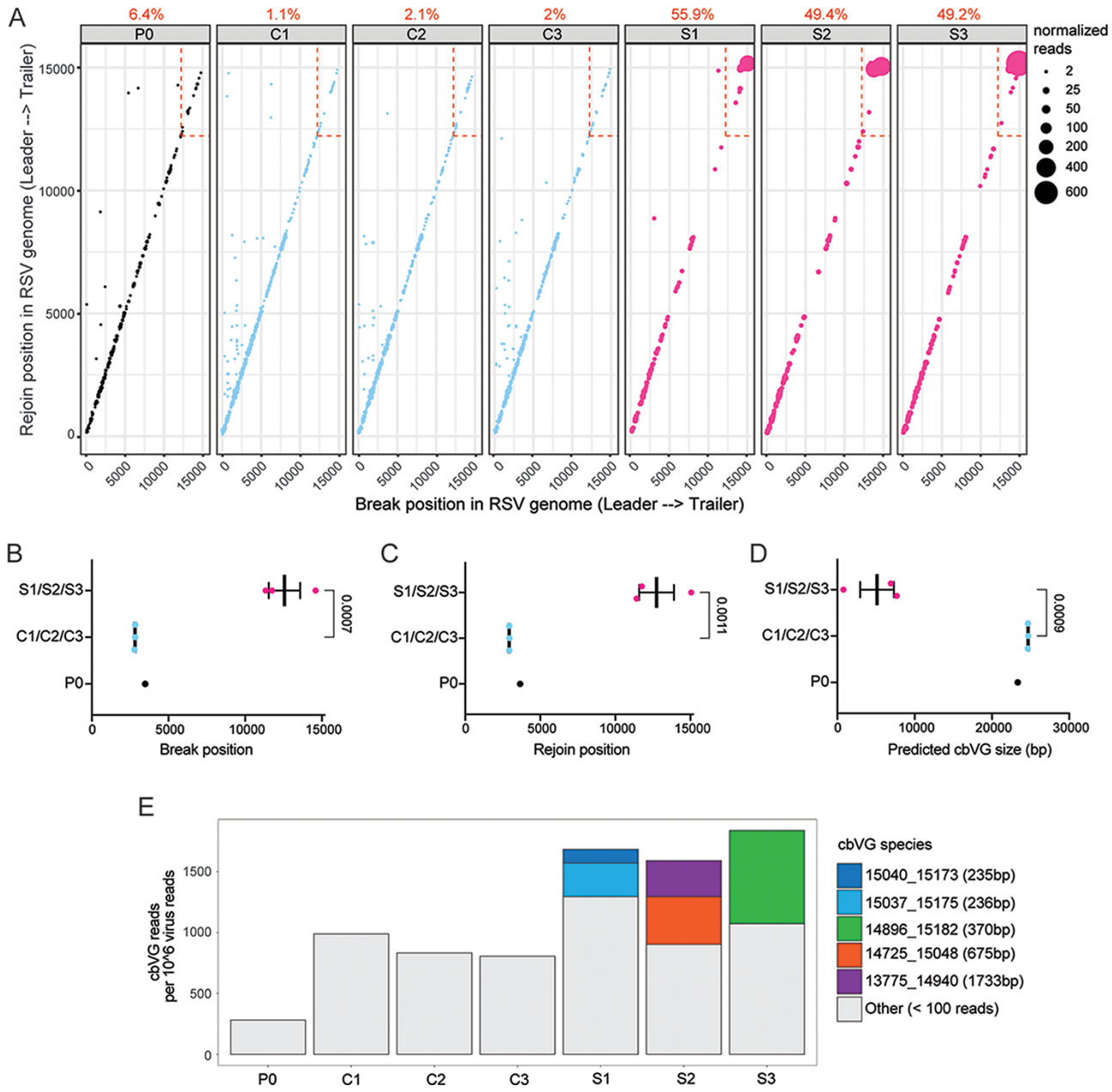

Figure 2. cbVG species in A549 control and A549 STAT1 KO cells at Passage 20. (A) Each dot represents a cbVG species and its break/rejoin position. The size of the dots represents the number of normalized reads per 10^6 virus reads. The percentage of cbVG reads within the last 3000 bp of the RSV genome (dashed box) is indicated above each plot. (B-D) Mean break position, rejoin position, and predicted cbVG size are shown in these graphs. Each dot represents the median of a lineage. Data are shown as mean ± SEM. Significant *P* values for the two-tailed unpaired *t* test between A549 control and A549 STAT1 KO ($n = 3$ lineages) are indicated. (E) Stacked bar graph shows cbVG species with at least 100 reads present in each sample. The legend includes information on break position, rejoin position, and predicted cbVG size. cbVG species with less than 100 reads were grouped together as 'Others'.

species RT-PCR approach (Felt et al. 2021). We first extracted RNA from the nasal washes and analyzed them following our RNAseq/VODKA2 pipeline. We observed that cbVGs generated within the last 3000 bp of the genome (dashed box) were almost absent in the samples, and mostly cbVG species of longer predicted size were detected (Fig. 3 and Table 2). These results indicate that cbVGs species of a longer predicted length are also generated during natural infections and are the most predominant cbVG species. Overall, although cbVGs of longer predicted size do not accumulate as much as short cbVGs *in vitro* (Fig. 2A and E), these newly discovered species of cbVGs are predominant *in vivo* (Fig. 3) and associate with distinct clinical outcomes as reported in our previous study (Felt et al. 2021), emphasizing the importance of taken them in consideration when studying RSV cbVG populations.

3.4 Virus replication levels drive cbVG species selection

We next investigated what drives the difference in cbVG populations at Passage 20 between A549 control cells and A549 STAT1 KO cells. As cbVGs are dependent on the virus replication machinery

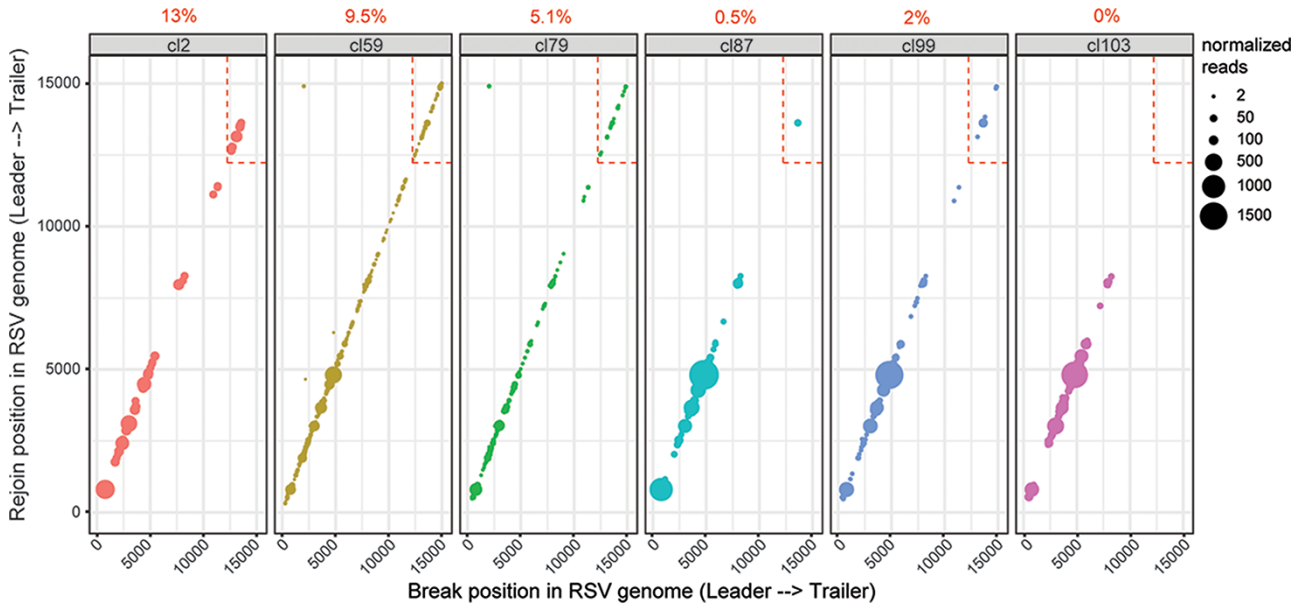

Figure 3. cbVGs in nasal washes of RSV-infected hospitalized pediatric patients. Each dot represents a cbVG species and its break/rejoin position. The size of the dots represents the number of normalized reads per 10^6 virus reads. The percentage of cbVG reads within the last 3000 bp of the RSV genome (dashed box) is indicated above each plot.

Table 2. RNAseq/VODKA2 data of clinical samples.

Sample	Median break position (IQR)	Median rejoin position (IQR)	Median predicted cbVG size in bp (IQR)
cl2	3,286 (2222–5134)	3,352 (2300–5170)	23,835 (20160–25942)
cl59	9,3661 (2249–4935)	3,705 (2333–4982)	23,017 (20526–25828)
cl79	2,981 (2000–4226)	3,030 (2032–4267)	24,445 (21969–26428)
cl87	4,361 (3014–4794)	4,377 (3031–4820)	21,726 (20854–24422)
cl99	4,582 (3556–4794)	4,608 (3589–4820	21,275 (20854–23317)
cl103	3,892 (3027–4794)	3,923 (3060–4821)	22,655 (20854–24370)

IQR = interquartile range

to be generated and replicated, we hypothesized that STAT1 exerts selective pressure on cbVGs by limiting virus replication and thereby driving their evolution within a virus population. To determine how cbVG populations evolved over time in control and STAT1 KO cells, we analyzed Passages 0, 4, 8, 12, 16, and 20 using our RNAseq/VODKA2 pipeline for all three lineages.

To assess this hypothesis, we first compared virus replication kinetics to the cbVG population diversity (Shannon's Entropy) kinetics in control and STAT1 KO cells using virus read as a proxy for replication (Fig. 4A and B). We noticed that cbVG population diversity kinetics followed the same pattern than virus replication kinetics (Fig. 4A and B). These data also show that a permissive host environment, such as STAT1 KO cells, that allows RSV replication to be sustained at high levels will promote a more diverse cbVG population early on (Passages 4, 8, and 12). As Shannon's entropy takes in consideration both richness (number of species present in a population) and evenness (relative abundance of each species in a population), we also analyzed cbVG species richness kinetics and the proportion of cbVGs within the last 3000 bp of the RSV genome over time. We observed that cbVG species richness kinetics also followed virus replication kinetics and that RSV generated more cbVG species early on (Passages 4, 8, and 12) in STAT1 KO cells (Fig. 4C). Interestingly, at Passages 16 and 20, Shannon's entropy and cbVG species richness dropped significantly in STAT1 KO cells and were even lower than control cells. To understand this observation, we next looked at the proportion of cbVGs within the last 3000 bp of the RSV genome (= predicted short cbVGs) (Fig. 4D). We measured this proportion in two ways: (1) percentage of predicted short cbVG species found in the sample (empty circles) and (2) percentage of predicted short cbVG reads found in the sample (full circles). In STAT1 KO cells, at Passages 16 and 20, RSV generated more of the shorter cbVGs species (empty circles) that also accumulated significantly (full circles) (Fig. 4D). These data suggest that predicted shorter cbVGs outcompeted the predicted longer cbVG species, which led to the drop in cbVG population diversity and richness in STAT1 KO cells at Passages 16 and 20. Importantly, only when the predicted short cbVGs predominated the cbVG population (Passage 20), we observed a significant increase in cbVG content in STAT1 KO cells (Fig. 4E). In rare circumstances, such as Passage 8 from control lineage 3, where virus reads dropped significantly, but a few cbVGs reads could still be detected (13 cbVG reads/6073 virus reads), cbVG content was also high in relationship to virus reads (Fig. 4E). Whether this is technical (e.g., threshold of detection) or biological (e.g., predicted long cbVGs are very stable in the absence of helper virus) is unknown. We also tracked the most predominant cbVG species in the three STAT1 KO cell lineages and observed that they were not present at P0 and were detected first at Passage 16 (Fig. 4F–H). This result indicates that predicted shorter cbVGs were *de novo* generated before being selected and outcompeting other cbVGs.

Overall, these data show that longer predicted cbVG species are predominant in both cell lines until sustained high virus replication levels lead to diversification and generation of shorter cbVGs. In STAT1 KO cells, where high virus replication levels

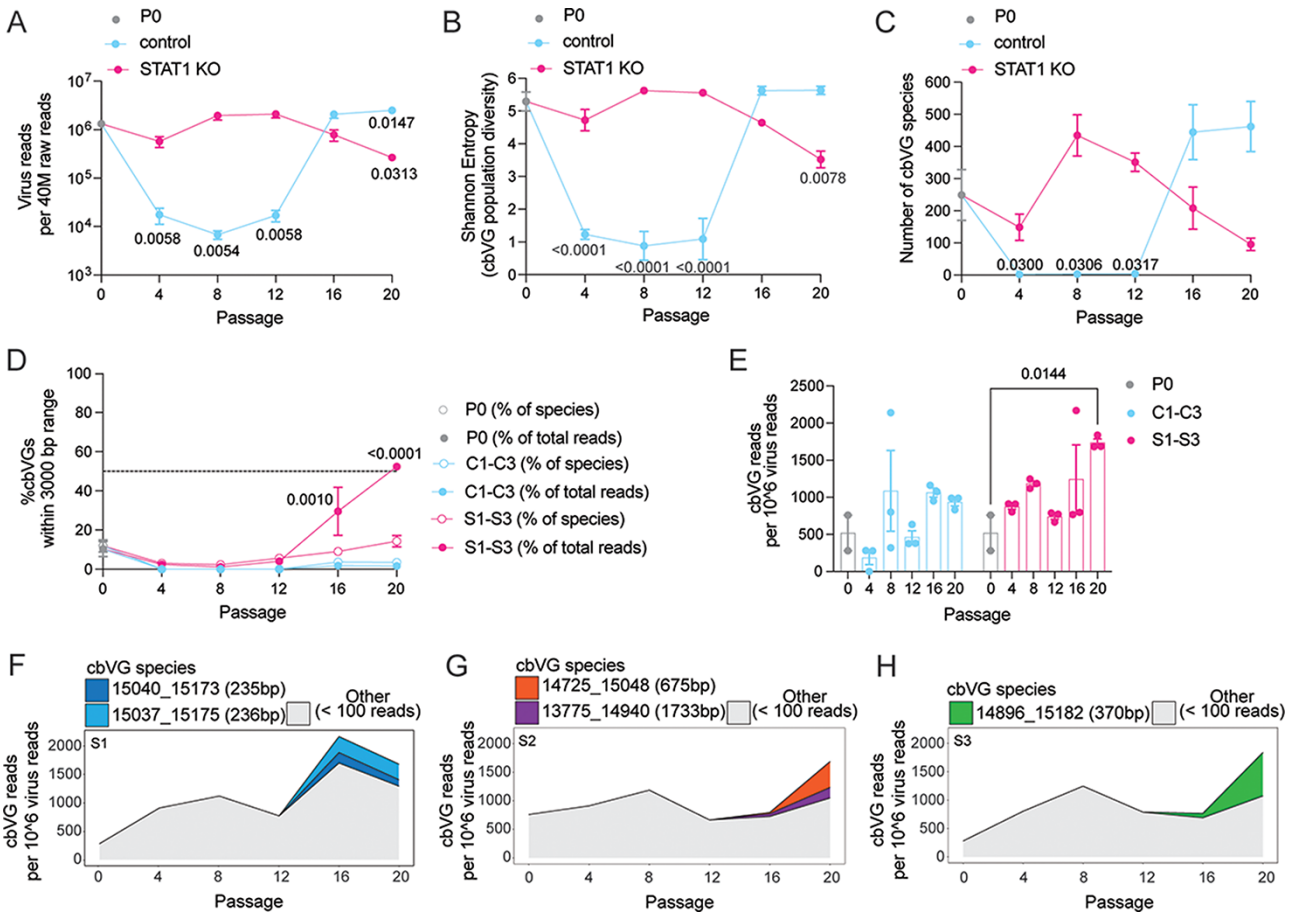

Figure 4. Sustained high replication levels in A549 STAT1 KO drive the selection of short cbVG species. (A) Line graph shows virus reads normalized per forty million total raw reads for different passages in A549 control or STAT1 KO cells. (B) Line graph shows Shannon's entropy for different passages in A549 control or STAT1 KO cells. Shannon's Entropy for each population was calculated using the formula $-\Sigma p_i \ln(p_i)$, where p_i is the relative abundance (proportion) of species i. (C) Line graph shows cbVG species richness for different passages in A549 control or STAT1 KO cells. (D) Line graph shows % cbVG species (empty circles) or reads (full circles) within the last 3000 bp of RSV genome for different passages in A549 control (blue) or STAT1 KO (pink) cells. (E) Bar graphs show cbVG reads normalized to one million virus reads. (A–E) Data are shown as mean ± SEM. *P* values for two-way analysis of variance (ANOVA) with the Bonferroni *post hoc* test comparing all passages ($n = 3$ lineages) to P0 ($n = 2$). (F-H) Continuous stacked bar graph shows cbVG species with at least 100 reads present in each sample of lineage 1, 2, and 3 of A549 STAT1 KO. The legend includes information on break position, rejoin position and predicted cbVG size. cbVG species with less than 100 reads were grouped together as 'Others'.

were maintained throughout the experiment, we observed that shorter cbVGs were selected and accumulated, which allowed for an increase in the overall cbVG content within the virus population. However, in control cells, this selection was not observed, likely because high virus replication levels were not maintained throughout the experiment and peak virus replication levels were not reached before Passage 20.

To more directly address if virus replication levels are the major driver of cbVG selection, we serially passaged RSV at a fixed MOI of either 0.1 or 10 in both A549 control and STAT1 KO cells for ten passages. As opposed to the fixed-volume experiment, these conditions would normalize virus replication levels between control and STAT1 KO cells throughout the experiment. A MOI of 0.1 was chosen to maintain virus replication levels low, and a MOI of 10 was chosen to maintain virus replication levels high. As with the fixed-volume experiment (Fig. 1A), we carried out three experimental evolution replicates for each cell line. We hypothesized that if sustained high replication levels is the major driver of short cbVG selection, we should observe selection of short cbVGs only at a fixed MOI of 10 in both cell lines due to normalization of virus replication levels.

As expected, RSV replication levels, as measured by titer, were similar between control and STAT1 KO cells throughout the experiment for both MOIs (Fig. 5A and B). We analyzed P0 and P10 viral stocks using the RNAseq/VODKA2 pipeline and found that RSV populations contained more cbVGs when passaged at an MOI of 10 than 0.1 in both cell lines (Fig. 5C). At a MOI of 10, we noticed an accumulation of cbVGs with break and rejoins occurring in the last 3000 bp of the RSV genome (dashed box) corresponding to cbVGs of short length regardless of the cell line (Fig. 5D). This accumulation did not occur at an MOI of 0.1 where mainly longer cbVGs were present (Fig. 5D). To assess if the differences observed were consistent between lineages, we plotted the median break, rejoin, and predicted size values for each lineage in each condition (Fig. 5E–G). All three analyses showed more drastic differences between MOIs of 0.1 and 10 than among control and STAT1 KO cells, which we expected due to normalization of virus replication levels between cell lines (Fig. 5E–G). At a MOI of 10, we noticed selection of shorter cbVG species that dominated the cbVG population (Fig. 5H), similar to what we observed in STAT1 KO in the fixed-volume experiment (Fig. 2E). Notably, at Passage 10, some of the most predominant cbVGs species were of longer predicted

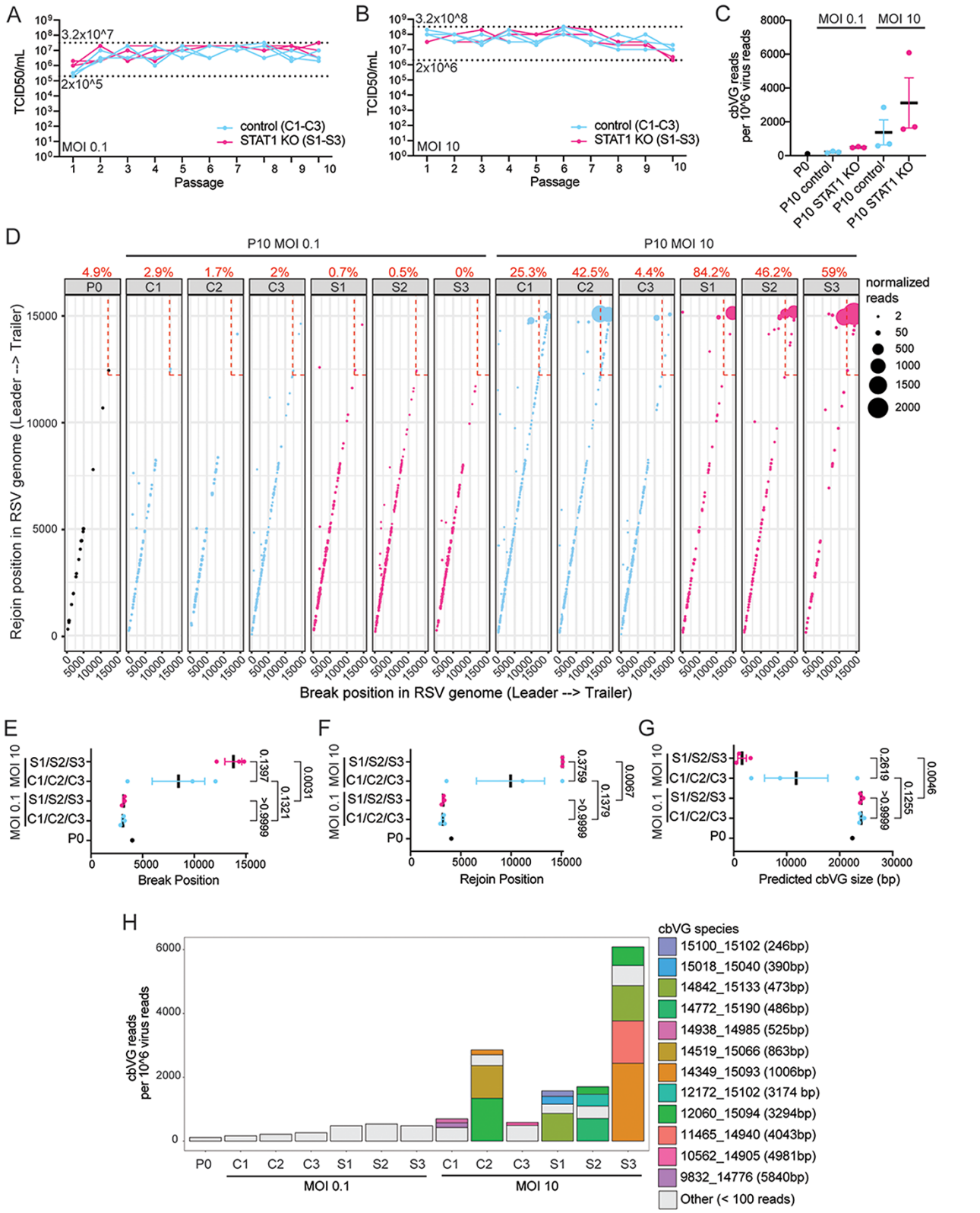

Figure 5. Selection of short cbVG species only occurs at high MOI conditions. (A and B) TCID50 assay was performed on Hep2 cells for all samples from fixed-MOI 0.1 and 10 experiment. Dashed lines indicate the minimum and maximum $TCID_{50}$/ml values reached in each experiment. (C) cbVG reads detected by VODKA2 were normalized per 10^6 virus reads. Each dot represents the median of a lineage. Data are shown as mean ± SEM. (D) Each dot represents a cbVG species and its break/rejoin position. The size of the dots represents the number of normalized reads per 10^6 virus reads. The percentage of cbVG reads within the last 3000 bp of the RSV genome (dashed box) is indicated above each plot. (E-G) Mean break position, rejoin position and predicted cbVG size are shown in these graphs. Each dot represents the median of a lineage. Data are shown as mean ± SEM. *P* values for one-way analysis of variance with the Bonferroni *post hoc* test for all groups are indicated. (H) Stacked bar graph shows cbVG species with at least 100 reads present in each sample. The legend includes information on break position, rejoin position, and predicted cbVG size. cbVG species with less than 100 reads were grouped together as 'Others'.

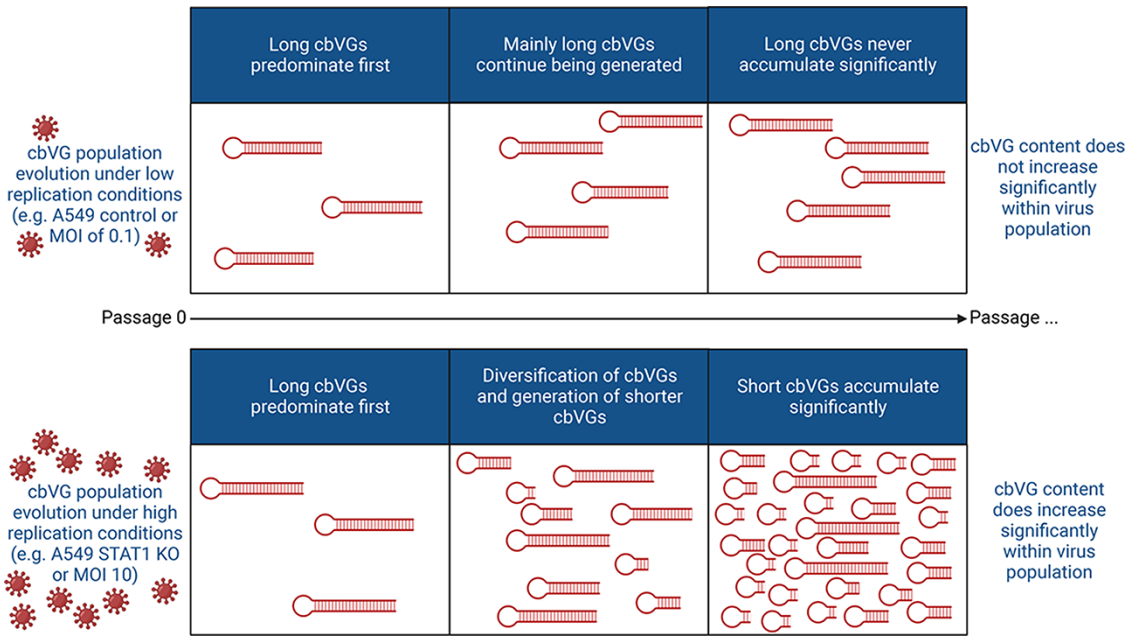

Figure 6. Schematic summary of cbVG population evolution in resistant and permissive hosts. Summary of the cbVG population changes observed in our study over time in different host environments.

length than the most predominant species at Passage 20 in the fixed-volume experiment, suggesting that the average length of accumulated cbVG species gets shorter over time (Figs 2E and 5H). Finally, we did observe that shorter cbVG species tended to accumulate more in STAT1 KO than control cells during the MOI of 10 passages, suggesting that other factors might play a minor role alongside virus replication levels (Fig. 5D–H).

We also compared the fixed-volume versus fixed-MOI experiments more directly (Fig. S2). Virus titers in the fixed-volume control and MOI of 0.1 experiments never went above 2×10^7 $TCID_{50}$/mL (see the dashed line); however, in the fixed-volume STAT1 KO and MOI 10 experiments, virus titers were sustained above this threshold over longer time periods (Fig. S2A). We also compared the distribution of break, rejoin, and size between the two experiments and observed a shift in distribution only in the fixed-volume STAT1 KO and MOI 10 experiments (Fig. S2B–S2C). These data again emphasize how virus replication levels need to be sustained above a certain threshold to generate and accumulate predicted shorter cbVGs.

Taken together, these data confirm that sustained high MOI (high replication) conditions are a main driver of the generation and selection of short cbVGs that accumulate within virus populations. We also show that more resistant cell lines, such as A549 control, which were not susceptible to cbVG accumulation in the fixed-volume experiment, can accumulate cbVGs if saturated by high MOI conditions. Meanwhile, the more permissive cell line A549 STAT1 KO, which was susceptible to cbVG accumulation in the fixed-volume experiment, does not accumulate cbVGs if MOI conditions are maintained to very low levels.

4. Discussion

Although nonstandard viral genomes play a crucial role in shaping virus infection outcomes (Sun et al. 2015; Vasilijevic et al. 2017; Felt et al. 2021), the principles that drive the selection and evolution of non standard viral genomes within a virus population are poorly understood. *In vitro*, nonstandard viral genomes usually accumulate within virus populations when RNA viruses are serially passaged at a high MOI (Von Magnus 1951; 1954; Kingsbury, Portner, and Darlington 1970; Stampfer, Baltimore, and Huang 1971; Huang 1973; Thompson and Yin 2010; Sun and Lopez 2016; Welch et al. 2020). These studies suggest that accumulation of nonstandard viral genomes is favored by increasing the number of cells infected, the virus replication within cells, and/or the number of co-infected cells with standard and nonstandard viral genomes. However, how nonstandard viral genome populations change when an increase in the cbVG content of a virus population occurs remains unknown.

Nonstandard viral genomes of the copy-back type are historically described as significantly shorter than standard viral genomes (Huang and Wagner 1966; Kingsbury, Portner, and Darlington 1970; Huang 1973; Lazzarini, Keene, and Schubert 1981; Vignuzzi and Lopez 2019), and it is unclear if the bias for a shorter size is due to preferential generation of short cbVGs, faster replication rate and accumulation of short cbVGs, and/or due to limitations in detection methods. It is also not clear how cbVG species are selected for under different environmental conditions and how this selection impacts the evolution of the overall cbVG population. In this study, we addressed how cbVG selection and cbVG population evolution are affected by a permissive host environment that allows sustained high replication levels (A549 STAT1 KO cells) or a resistant host environment that limits replication levels (A549 control cells). Overall, we found that cbVGs of a longer predicted size predominate first and that sustained high RSV replication levels lead to cbVG population diversification. This diversification primes the generation and selection of shorter cbVGs that later accumulate and allow for an increase in the cbVG content within a virus population (Fig. 6).

It is important to note that although permissive STAT1 KO cells accumulated significantly more cbVGs than resistant control cells, cbVGs were found in both cell lines (Fig. 1B and Table 1). These data suggest that accumulation but not generation of cbVGs is dependent on sustained high virus replication. This is consistent with our recent study where we showed that cbVGs were found

in nasal washes of experimentally RSV-infected adult patients before high virus replication levels were reached (Felt et al. 2021). Taken together, our study also shows that the generation of cbVGs is inherent to RSV replication and that most RSV populations will contain cbVGs. This is likely true for many other RNA viruses and, as cbVGs have been shown to play a crucial role in virus infections, our data underlines the need to consider cbVGs in the study of RNA virus populations.

Next-generation sequencing and pipelines to analyze virus populations have improved significantly in recent years (Routh and Johnson 2014; Timm, Akpinar, and Yin 2014; Jaworski and Routh 2017; Beauclair et al. 2018; Bosma et al. 2019; Boussier et al. 2020; Olmo-Uceda et al. 2022). In this study, we used an updated version of our previously published RNAseq/VODKA pipeline, called VODKA2, to study cbVG populations (Sun et al. 2019). Previous methods such as RT-PCR more efficiently detect short cbVGs that are of high abundance; however, our RNAseq/VODKA2 pipeline can overcome these challenges and detect unbiasedly cbVG species of various predicted sizes and abundance (Fig. 2A). Therefore, VODKA2 revealed that the diversity of cbVGs generated by RSV is much larger than previously thought. The use of stranded total RNA library preparation kits can further allow VODKA2 to determine if cbVGs are only generated (only genomic) or are also being replicated by the viral polymerase (mixture of genomic and antigenomic). From a stranded library preparation on P0, P20 C1–C3, and P20 S1–S3, we were able to determine that 39.77 per cent of cbVGs were genomic and 60.23 per cent of cbVGs were antigenomic, indicating that cbVGs were not only generated but also replicated (Fig. S3). Furthermore, short cbVGs (especially shorter than 6000 bp) correlated with more reads. indicating that short cbVGs are more likely to replicate more efficiently as has been shown previously for some nonstandard viral genomes (Fig. S4) (Laske et al. 2016; Mendes and Russell 2021; Pelz et al. 2021). Overall, these data suggest that sustained high replication drives the generation of shorter cbVGs; however, it is likely that the highly efficient replication of short cbVGs ultimately leads to their accumulation and an overall increase in the cbVG content within a virus population.

Our RNAseq/VODKA2 pipeline also allowed us to compare cbVG species between virus populations from the cell line that limited virus replication (A549 control cells) and the cell line that allowed high virus replication (A549 STAT1 KO cells). The virus population observed in STAT1 KO cells mainly consisted of shorter cbVGs, whereas the virus population from control cells consisted mainly of much longer cbVGs. A fixed-MOI passaging experiment confirmed that it was sustained high virus replication levels that drive the selection of shorter versus longer cbVGs. In the fixed-volume passaging experiment, we observed that sustained high virus replication over several passages drives cbVG diversification and generation of short cbVGs that will significantly accumulate (Fig. 4). This demonstrates that high virus replication does not directly lead to cbVG accumulation and instead requires an intermediate step that consists of cbVG diversification and generation of short cbVGs, which then accumulate and take over the cbVG population (Fig. 6). The exact molecular mechanism that drives the generation of shorter cbVGs is not clear. Are shorter cbVGs generated from longer ones? Do high virus replication levels affect the processivity of the polymerase directly or maybe indirectly through host factors? Future studies will address these questions.

In this study, we also discovered the first evidence of cbVGs of long predicted sizes. These cbVGs are predominant at first *in vitro* and are the most predominant *in vivo*. Some of these cbVGs are predicted to be longer than the genome (Fig. S1B). It is possible that previous studies did not detect these longer cbVGs due to lack of sensitivity in the methods used. The fact that we detected these longer cbVGs in patients raises the question on how they are functionally different from the shorter cbVGs, which have been studied so far *in vitro*. Do they interact with different pattern recognition receptors and/or induce different signaling pathways? Why do we mainly find longer cbVGs in patients and less shorter ones? Is there a fitness advantage of these longer cbVGs *in vivo*? We must also consider that we are limited to nasal samples from patients and that cbVG populations could differ between microenvironments (e.g., nose vs. lung) as has been shown for Zika nonstandard viral genomes (Johnson et al. 2020). However, we have observed that Sendai virus (SeV) populations in the lung of mice also consist of mainly longer cbVGs, indicating that this might be a common feature of *in vivo* cbVG populations (unpublished data). Further characterization of longer cbVGs is still needed as we can only extract predicted sizes based on VODKA2. Due to their size and complex structure, amplifying or sequencing the entire sequence of long cbVGs by RT-PCR or MinION remains a challenge. So far, we were able to confirm that the junction regions at least are not artifactual as we did not detect copy-backs when running VODKA2 using a RSV database (negative control for false positivity rate of VODKA2) or Glyceraldehyde 3-phosphate dehydrogenase/actin databases (negative controls for library prep generating copy-back sequences) on SeV samples (Fig. S5A). Interestingly, cbVG species of longer predicted size never accumulated to significant amounts, strongly suggesting that they are indeed of longer size and hence not as competitive against the standard viral genome or shorter cbVG species (Fig. S4). However, it is important to note that many predicted long cbVG species can be detected in several passages and follow virus kinetics, which suggests that they could potentially be replicated and packaged (Fig. S5B).

Nonstandard viral genomes can interfere with standard viral genome replication when they accumulate to significant levels causing a significant drop in infectious virus particles (Palma and Huang 1974; Kirkwood and Bangham 1994; Manzoni and Lopez 2018; Genoyer and Lopez 2019). Although cbVGs did accumulate to significant levels in STAT1 KO cells, we did not observe such a significant decrease in infectious virus particles in the fixed-volume experiment (Fig. 1B). This is likely due to cbVGs being less interfering in the absence of antiviral responses (e.g., mediated by STAT1), such as has been shown for RSV and parainfluenza virus 5 (Sun et al. 2015; Wignall-Fleming et al. 2020).

Currently, they are few studies showing what roles host proteins could play in nonstandard viral genome generation, accumulation, and selection (Holland, Villarreal, and Breindl 1976; Kang and Allen 1978). We have previously shown that children are more likely to accumulate RSV cbVGs than adults and that female patients are more likely to accumulate RSV cbVGs than males (Felt et al. 2021). Furthermore, in an adult cohort, although all patients were experimentally infected with the same virus (RSV Memphis 37), not all patients accumulated cbVGs (Felt et al. 2021). All these studies strongly suggest that the host might play an important role in shaping cbVG populations. In this study, we have shown that STAT1 by limiting virus replication can exert selective pressure on cbVG populations and shape their evolution. It will be important to assess in future studies what other host proteins can shape cbVG content within virus populations.

Data availability

Raw sequence data are deposited on SRA (PRJNA837014).

Supplementary data

Supplementary data are available at *Virus Evolution* online.

Acknowledgements

We thank Dr. Susan Weiss for kindly providing A549 control and STAT1 KO cells. Figs. 1A, S1A, and S6 were created with BioRender.com.

Funding

This work was supported by the U.S. National Institutes of Health National Institute of Allergy and Infectious Diseases (AI137062 and AI134862 to CLB).

Conflict of interest: None declared.

References

Baum, A., Sachidanandam, R., and Garcia-Sastre, A. (2010) 'Preference of RIG-I for Short Viral RNA Molecules in Infected Cells Revealed by Next-generation Sequencing', *Proceedings of the National Academy of Sciences of the United States of America*, 107: 16303–8.

Beauclair, G. et al. (2018) 'DI-tector: Defective Interfering Viral Genomes' Detector for Next-generation Sequencing Data', *RNA*, 24: 1285–96.

Bosma, T. J. et al. (2019) 'Identification and Quantification of Defective Virus Genomes in High Throughput Sequencing Data Using DVG-profiler, a Novel Post-sequence Alignment Processing Algorithm', *PLoS One*, 14: e0216944.

Boussier, J. et al. (2020) 'RNA-seq Accuracy and Reproducibility for the Mapping and Quantification of Influenza Defective Viral Genomes', *RNA*, 26: 1905–18.

Carrasco-Hernandez, R. et al. (2017) 'Are RNA Viruses Candidate Agents for the Next Global Pandemic? A Review', *ILAR Journal/National Research Council, Institute of Laboratory Animal Resources*, 58: 343–58.

Collins, P. L., Fearns, R., and Graham, B. S. (2013) 'Respiratory Syncytial Virus: Virology, Reverse Genetics, and Pathogenesis of Disease', *Current Topics in Microbiology and Immunology*, 372: 3–38.

Durbin, J. E. et al. (2002) 'The Role of IFN in Respiratory Syncytial Virus Pathogenesis', *Journal of Immunology (Baltimore, Md.: 1950)*, 168: 2944–52.

Felt, S. A. et al. (2021) 'Detection of Respiratory Syncytial Virus Defective Genomes in Nasal Secretions Is Associated with Distinct Clinical Outcomes', *Nature Microbiology*, 6: 672–81.

Genoyer, E. and Lopez, C. B. (2019) 'Defective Viral Genomes Alter How Sendai Virus Interacts with Cellular Trafficking Machinery, Leading to Heterogeneity in the Production of Viral Particles among Infected Cells', *Journal of Virology*, 93.

González-Aparicio, L. J., López, C. B., and Felt, S. A. (2022) 'A Virus Is a Community: Diversity within Negative-Sense RNA Virus Populations', *Microbiology and Molecular Biology Reviews*, 86: e0008621.

Hashimoto, K. et al. (2005) 'Respiratory Syncytial Virus Infection in the Absence of STAT 1 Results in Airway Dysfunction, Airway Mucus, and Augmented IL-17 Levels', *The Journal of Allergy and Clinical Immunology*, 116: 550–7.

Henle, W., and Henle, G. (1943) 'Interference of Inactive Virus with the Propagation of Virus of Influenza', *Science*, 98: 87–9.

Ho, T. H. et al. (2016) 'PACT- and RIG-I-Dependent Activation of Type I Interferon Production by a Defective Interfering RNA Derived from Measles Virus Vaccine', *Journal of Virology*, 90: 1557–68.

Holland, J. J., Villarreal, L. P., and Breindl, M. (1976) 'Factors Involved in the Generation and Replication of Rhabdovirus Defective T Particles', *Journal of Virology*, 17: 805–15.

Huang, A. S. (1973) 'Defective Interfering Viruses', *Annual Review of Microbiology*, 27: 101–17.

Huang, A. S., and Wagner, R. R. (1966) 'Comparative Sedimentation Coefficients of RNA Extracted from Plaque-forming and Defective Particles of Vesicular Stomatitis Virus', *Journal of Molecular Biology*, 22: 381–4.

Jaworski, E., and Routh, A. (2017) 'Parallel ClickSeq and Nanopore Sequencing Elucidates the Rapid Evolution of Defective-interfering RNAs in Flock House Virus', *PLoS Pathogens*, 13: e1006365.

Johnson, K. E. E. et al. (2020) 'Mapping the Evolutionary Landscape of Zika Virus Infection in Immunocompromised Mice', *Virus Evolution*, 6: veaa092.

Kang, C. Y., and Allen, R. (1978) 'Host Function-dependent Induction of Defective Interfering Particles of Vesicular Stomatitis Virus', *Journal of Virology*, 25: 202–6.

Kingsbury, D. W., Portner, A., and Darlington, R. W. (1970) 'Properties of Incomplete Sendai Virions and Subgenomic Viral RNAs', *Virology*, 42: 857–71.

Kirkwood, T. B., and Bangham, C. R. (1994) 'Cycles, Chaos, and Evolution in Virus Cultures: A Model of Defective Interfering Particles', *Proceedings of the National Academy of Sciences of the United States of America*, 91: 8685–9.

Kolakofsky, D. (1976) 'Isolation and Characterization of Sendai Virus DI-RNAs', *Cell*, 8: 547–55.

Laske, T. et al. (2016) 'Modeling the Intracellular Replication of Influenza A Virus in the Presence of Defective Interfering RNAs', *Virus Research*, 213: 90–9.

Lazzarini, R. A., Keene, J. D., and Schubert, M. (1981) 'The Origins of Defective Interfering Particles of the Negative-strand RNA Viruses', *Cell*, 26: 145–54.

Li, T., and Pattnaik, A. K. (1997) 'Replication Signals in the Genome of Vesicular Stomatitis Virus and Its Defective Interfering Particles: Identification of a Sequence Element that Enhances DI RNA Replication', *Virology*, 232: 248–59.

Linder, A. et al. (2021) 'Defective Interfering Genomes and the Full-Length Viral Genome Trigger RIG-I after Infection with Vesicular Stomatitis Virus in a Replication Dependent Manner', *Frontiers in Immunology*, 12: 595390.

Liu, S. et al. (2021) 'Critical Role of Syk-dependent STAT1 Activation in Innate Antiviral Immunity', *Cell Reports*, 34: 108627.

Manzoni, T. B., and Lopez, C. B. (2018) 'Defective (Interfering) Viral Genomes Re-explored: Impact on Antiviral Immunity and Virus Persistence', *Future Virology*, 13: 493–503.

Mendes, M., and Russell, A. B. (2021) 'Library-based Analysis Reveals Segment and Length Dependent Characteristics of Defective Influenza Genomes', *PLoS Pathogens*, 17: e1010125.

Mesev, E. V., LeDesma, R. A., and Ploss, A. (2019) 'Decoding Type I and III Interferon Signalling during Viral Infection', *Nature Microbiology*, 4: 914–24.

Mura, M. et al. (2017) 'Nonencapsidated 5′ Copy-Back Defective Interfering Genomes Produced by Recombinant Measles Viruses are Recognized by RIG-I and LGP2 but Not MDA5', *Journal of Virology*, 91.

Olmo-Uceda, M. J. et al. (2022) 'DVGfinder: A Metasearch Engine for Identifying Defective Viral Genomes in RNA-Seq Data', *Viruses*, 14: 1114.

Palma, E. L., and Huang, A. (1974) 'Cyclic Production of Vesicular Stomatitis Virus Caused by Defective Interfering Particles', *The Journal of Infectious Diseases*, 129: 402–10.

Pelz, L. et al. (2021) 'Semi-continuous Propagation of Influenza A Virus and Its Defective Interfering Particles: Analyzing the Dynamic Competition to Select Candidates for Antiviral Therapy', *Journal of Virology*, 95: e0117421.

Rao, D. D., and Huang, A. S. (1982) 'Interference among Defective Interfering Particles of Vesicular Stomatitis Virus', *Journal of Virology*, 41: 210–21.

Routh, A., and Johnson, J. E. (2014) 'Discovery of Functional Genomic Motifs in Viruses with ViReMa-a Virus Recombination Mapper-for Analysis of Next-generation Sequencing Data', *Nucleic Acids Research*, 42: e11.

Runge, S. et al. (2014) 'In Vivo Ligands of MDA5 and RIG-I in Measles Virus-infected Cells', *PLoS Pathogens*, 10: e1004081.

Santak, M. et al. (2015) 'Accumulation of Defective Interfering Viral Particles in Only a Few Passages in Vero Cells Attenuates Mumps Virus Neurovirulence', *Microbes and Infection/Institut Pasteur*, 17: 228–36.

Stampfer, M., Baltimore, D., and Huang, A. S. (1971) 'Absence of Interference during High-multiplicity Infection by Clonally Purified Vesicular Stomatitis Virus', *Journal of Virology*, 7: 409–11.

Stier, M. T. et al. (2017) 'STAT1 Represses Cytokine-Producing Group 2 and Group 3 Innate Lymphoid Cells during Viral Infection', *Journal of Immunology (Baltimore, Md. : 1950)*, 199: 510–9.

Strahle, L., Garcin, D., and Kolakofsky, D. (2006) 'Sendai Virus Defective-interfering Genomes and the Activation of Interferon-beta', *Virology*, 351: 101–11.

Strahle, L. et al. (2007) 'Activation of the Beta Interferon Promoter by Unnatural Sendai Virus Infection Requires RIG-I and Is Inhibited by Viral C Proteins', *Journal of Virology*, 81: 12227–37.

Sun, Y., and Lopez, C. B. (2016) 'Preparation of Respiratory Syncytial Virus with High or Low Content of Defective Viral Particles and Their Purification from Viral Stocks', *Bio Protocol*, 6.

Sun, Y. et al. (2015) 'Immunostimulatory Defective Viral Genomes from Respiratory Syncytial Virus Promote a Strong Innate Antiviral Response during Infection in Mice and Humans', *PLoS Pathogens*, 11: e1005122.

—— et al. (2019) 'A Specific Sequence in the Genome of Respiratory Syncytial Virus Regulates the Generation of Copy-back Defective Viral Genomes', *PLoS Pathogens*, 15: e1007707.

Tapia, K. et al. (2013) 'Defective Viral Genomes Arising in Vivo Provide Critical Danger Signals for the Triggering of Lung Antiviral Immunity', *PLoS Pathogens*, 9: e1003703.

Thompson, K. A., and Yin, J. (2010) 'Population Dynamics of an RNA Virus and Its Defective Interfering Particles in Passage Cultures', *Virology Journal*, 7: 257.

Tilston-Lunel, N. L. et al. (2021) 'Sustained Replication of Synthetic Canine Distemper Virus Defective Genomes In Vitro and In Vivo', *mSphere*, 6: e0053721.

Timm, C., Akpinar, F., and Yin, J. (2014) 'Quantitative Characterization of Defective Virus Emergence by Deep Sequencing', *Journal of Virology*, 88: 2623–32.

Treuhaft, M. W., and Beem, M. O. (1982) 'Defective Interfering Particles of Respiratory Syncytial Virus', *Infection and Immunity*, 37: 439–44.

Vasilijevic, J. et al. (2017) 'Reduced Accumulation of Defective Viral Genomes Contributes to Severe Outcome in Influenza Virus Infected Patients', *PLoS Pathogens*, 13: e1006650.

Vignuzzi, M., and Lopez, C. B. (2019) 'Defective Viral Genomes are Key Drivers of the Virus-host Interaction', *Nature Microbiology*, 4: 1075–87.

Von Magnus, P. (1951) 'Propagation of the PR8 Strain of Influenza A Virus in Chick Embryos. II. The Formation of Incomplete Virus following Inoculation of Large Doses of Seed Virus', *Acta Pathologica Et Microbiologica Scandinavica*, 28: 278–93.

—— (1954) 'Incomplete Forms of Influenza Virus', *Advances in Virus Research*, 2: 59–79.

Welch, S. R. et al. (2020) 'Inhibition of Nipah Virus by Defective Interfering Particles', *The Journal of Infectious Diseases*, 221: S460–7.

Whelan, J. N. et al. (2019) 'Zika Virus Production Is Resistant to RNase L Antiviral Activity', *Journal of Virology*, 93.

Wignall-Fleming, E. B. et al. (2020) 'Innate Intracellular Antiviral Responses Restrict the Amplification of Defective Virus Genomes of Parainfluenza Virus 5', *Journal of Virology*, 94.

Williams, E. S. et al. (2016) 'Repeatable Population Dynamics among Vesicular Stomatitis Virus Lineages Evolved under High Co-infection', *Frontiers in Microbiology*, 7: 370.

Xu, J. et al. (2015) 'Identification of a Natural Viral RNA Motif that Optimizes Sensing of Viral RNA by RIG-I', *mBio*, 6: e01265–01215.

—— et al. (2017) 'Replication Defective Viral Genomes Exploit a Cellular Pro-survival Mechanism to Establish Paramyxovirus Persistence', *Nature Communications*, 8: 799.

Yount, J. S. et al. (2008) 'MDA5 Participates in the Detection of Paramyxovirus Infection and Is Essential for the Early Activation of Dendritic Cells in Response to Sendai Virus Defective Interfering Particles', *Journal of Immunology (Baltimore, Md. : 1950)*, 180: 4910–8.